










Semi-Quantitative Analysis for Determining the Optimal Threshold Value on CT to Measure the Solid Portion of Pulmonary Subsolid Nodules

폐의 아고형결절에서 침습적 병소를 검출하기 위한 반-정량 분석을 통한 최적의 CT 임계 값 결정

Sunyong Lee, MD¹ , Da Hyun Lee, MD¹ , Jae Ho Lee, MD¹ ,
Sungsoo Lee, MD² , Kyunghwa Han, PhD³ ,
Chul Hwan Park, MD¹ , Tae Hoon Kim, MD^{1*} 

¹Department of Radiology and the Research Institute of Radiological Science, Gangnam Severance Hospital, Yonsei University College of Medicine, Seoul, Korea

²Department of Thoracic and Cardiovascular Surgery, Gangnam Severance Hospital, Yonsei University College of Medicine, Seoul, Korea

³Department of Radiology, Research Institute of Radiological Science, Severance Hospital, Yonsei University College of Medicine, Seoul, Korea

Purpose This study aimed to investigate the optimal threshold value in Hounsfield units (HU) on CT to detect the solid components of pulmonary subsolid nodules using pathologic invasive foci as reference.

Materials and Methods Thin-section non-enhanced chest CT scans of 25 patients with pathologically confirmed minimally invasive adenocarcinoma were retrospectively reviewed. On CT images, the solid portion was defined as the area with higher attenuation than various HU thresholds ranging from -600 to -100 HU in 50-HU intervals. The solid portion was measured as the largest diameter on axial images and as the maximum diameter on multiplanar reconstruction images. A linear mixed model was used to evaluate bias in each threshold by using the pathological size of invasive foci as reference.

Results At a threshold of -400 HU, the biases were lowest between the largest/maximum diameter of the solid portion of subsolid nodule and the size of invasive foci of the pathological specimen, with 0.388 and -0.0176, respectively. They showed insignificant difference ($p = 0.2682$, $p = 0.963$, respectively) at a threshold of -400 HU.

Conclusion For quantitative analysis, -400 HU may be the optimal threshold to define the solid

Received April 6, 2020
Revised June 30, 2020
Accepted August 9, 2020






*Corresponding author

Tae Hoon Kim, MD
Department of Radiology and the Research Institute of Radiological Science, Gangnam Severance Hospital, Yonsei University College of Medicine, 211 Eonju-ro, Gangnam-gu, Seoul 06273, Korea.

Tel 82-2-2019-3510
Fax 82-2-3462-5472
E-mail thkim1@yuhs.ac

This is an Open Access article distributed under the terms of the Creative Commons Attribution Non-Commercial License (<https://creativecommons.org/licenses/by-nc/4.0>) which permits unrestricted non-commercial use, distribution, and reproduction in any medium, provided the original work is properly cited.

ORCID iDs

Sunyong Lee 
<https://orcid.org/0000-0001-7751-5465>
Da Hyun Lee 
<https://orcid.org/0000-0001-7593-0403>
Jae Ho Lee 
<https://orcid.org/0000-0002-8592-1209>
Sungsoo Lee 
<https://orcid.org/0000-0001-8998-9510>
Kyunghwa Han 
<https://orcid.org/0000-0002-5687-7237>
Chul Hwan Park 
<https://orcid.org/0000-0002-0004-9475>
Tae Hoon Kim 
<https://orcid.org/0000-0002-4032-1285>

portion of subsolid nodules as a surrogate marker of invasive foci.

Index terms Lung Neoplasms; Solitary Pulmonary Nodule; Adenocarcinoma of Lung; Multidetector Computed Tomography

INTRODUCTION

Subsolid nodules (SSNs), also known as ground-glass nodules, include nodules with hazy increased attenuation that do not obscure underlying bronchial structures or pulmonary vessels (1). The presence of a solid component in SSNs suggests its invasiveness and malignancy. Therefore, the presence and size of the solid portion are important for risk stratification and treatment planning (2, 3).

In the 2017 Fleischner guidelines, when the size of persistent SSNs with a solid component is more than 6 mm, malignancy is highly suspected compared to when the size is larger than 6 mm without a solid portion (2). According to the Lung CT Screening Reporting and Data System, SSNs with a solid component > 6 mm or a growing solid component are classified into category 4, whereas pure SSNs are categorized into category 2 or 3 (4). In lung cancer staging by the American Joint Committee on Cancer (8th edition), the largest diameter of a solid component of ground-glass nodules is measured on the multiplanar reconstruction (MPR) image, and diameters of up to 1, 2, and 3 cm are cT1a, cT1b, and cT1c, respectively (5).

Defining and measuring the solid portion of SSNs are important. However, defining SSNs is a challenging task (6, 7). Conventionally, it is based on the visual finding of individual assessment. Furthermore, the assessment of SSNs depends on the qualitative description from the individual radiologists with different CT scan protocols. Therefore, intra-observer and inter-observer variability among experienced chest radiologists cannot be avoided (8-10). Quantitative measurement of SSNs and its solid component may improve the accuracy and reduce inter-observer variability for differential diagnosis of SSNs. Few studies have evaluated the threshold attenuation for the solid portion indicating invasion foci on CT (11-13).

Despite these approaches, a quantitative threshold to determine the solid component of ground-glass nodules has not been established. Therefore, our study aimed to establish the optimal CT threshold value in Hounsfield units (HU) for detecting the solid components of SSNs.

MATERIALS AND METHODS

The study was approved by the Institutional Review Board of Gangnam Severance Hospital. Clinical data were reviewed from medical records (IRB No. 3-2016-0306). Given the retrospective nature of the study and the use of anonymized data, requirements for informed consent were waived.

PATIENTS

Twenty-five patients who underwent surgical resection of persistent SSNs and had patho-

logically confirmed minimally invasive adenocarcinoma (MIA) in Gangnam Severance Hospital were consecutively and retrospectively included. MIA was defined as lepidic-predominant adenocarcinoma measuring up to 3 cm with an invasive component measuring up to 0.5 cm and lacking lymphatic, vascular, alveolar space, or pleural invasion (5).

CT PROTOCOL

Standard CT images were acquired using two CT scanners: a 16-slice multidetector CT (MDCT) scanner (Somatom Sensation 16; Siemens Medical Solutions, Erlangen, Germany) and a 64-slice MDCT scanner (Somatom Sensation 64; Siemens Medical Solutions). Non-enhanced CT scan was performed at a tube potential of 120 kVp with automatic exposure control (100–200 mA). Axial images were reconstructed at a section width of 1 mm with 1-mm interval by filtered back projection technique and sharp convolution kernel.

CT IMAGE ANALYSIS

The solid components of SSN more than the cut off value were assumed to be direct surrogate markers to the invasive foci of pathologic specimen. The solid component of SSNs was defined as the area with high attenuation than a certain threshold in HU.

All pre-operative CT images of enrolled patients were analyzed with a commercial program (Aquarius iNtuition Ver. 4.4.12; TeraRecon, Inc., Foster City, CA, USA). The largest diameter of the solid portion is estimated on the axial image, and the maximum diameter of the solid portion is estimated on the MPR image in this program by setting a specific value and masking it in the lung window setting (W: 1400; L: -500) (Fig. 1). The diameter of lesions more than the threshold attenuation on each image was measured independently by two radiologists (C.P. and T.K), with 10 years and 25 years of experience in chest CT, respectively.

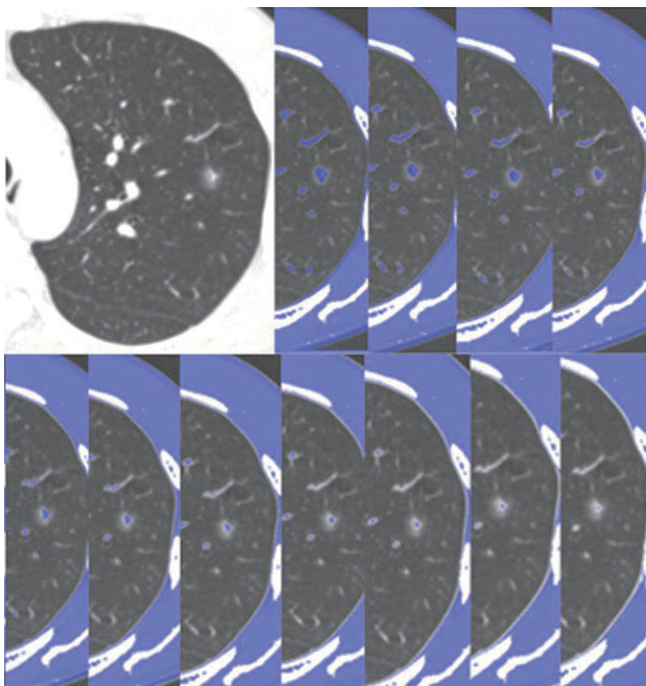


Fig. 1. Measurement of the largest diameter of the solid portion on axial images.

Lesions with higher than threshold attenuation are regarded as solid portions and marked with blue. The largest diameter is then measured by an individual. Threshold attenuation is arranged from the top left (-600 HU) to the bottom right (-100 HU). The largest diameter of the solid portion decreases as threshold attenuation increases.
HU = Hounsfield units

Various thresholds ranging from -600 to -100 HU were applied in 50-HU intervals.

CATEGORICAL ASSESSMENT

Twenty-five pathologically proven MIA SSNs were categorized into radiologic adenocarcinoma in situ (AIS), MIA, and invasive adenocarcinoma (IA) based on criteria of the measured solid portion on CT at each HU threshold from -600 HU to -100 HU: 0 mm, 0 mm to 5 mm, and larger than 5 mm. Classification was performed in both axial and MPR images, respectively.

STATISTICAL ANALYSIS

All continuous variables were expressed as mean \pm standard deviation. Categorical variables were summarized as frequencies or percentages. Data normality was evaluated using Shapiro-Wilk test. Bias between CT measurement of the solid portion and invasive foci on pathologic specimen was defined as the mean difference between the largest diameter of the solid component on the CT image and pathological invasive focus. It was evaluated with linear mixed model using Bonferroni's method for considering repeated measurements from various thresholds. Inter-observer reproducibility in measuring the solid portions on axial and MPR images was evaluated with the intraclass correlation coefficient. A *p* value < 0.05 was considered statistically significant. For analysis, R (version 3.3.1.; R Foundation for Statistical Computing, Vienna, Austria) was used.

RESULTS

PATIENT AND LESION CHARACTERISTICS

The mean age of the 25 patients was 55.9 ± 12.7 years. Seven male patients (28%) were included in this study. The mean size of SSN was 9.2 ± 1.33 mm, and the mean attenuation was -539.1 ± 96 HU. The mean size of invasive foci, confirmed by pathology, was 3.56 ± 1.33 mm.

SEMI-QUANTITATIVE CT ANALYSIS ON AXIAL AND MULTIPLANAR RECONSTRUCTED IMAGES

The largest size of the solid portion on the axial image at each HU threshold from -600 HU to -100 HU in 50 HU intervals is shown in Table 1. At a threshold of -400 HU on the axial image, the bias was lowest between the measured solid components of SSNs and pathologically confirmed invasive foci (0.388), showing insignificant difference ($p = 0.2682$) (Fig. 2).

The maximum size of the solid portion on the MPR image at each HU threshold from -600 HU to -100 HU in 50 HU intervals is shown in Table 1. Compared with the analysis on the axial image, the solid lesion component was larger on the MPR image. The measurements of solid components were not significantly different from the invasive component size on pathology at -400 HU threshold ($p = 0.963$). Similarly, at a threshold of -400 HU on the multiplanar reconstructed image, the bias was lowest (-0.0176) between the measured solid components of SSNs and pathologically confirmed invasive foci (Fig. 3). Inter-observer agreement in measuring the solid portion on axial and MPR images was excellent, with 0.985 and 0.961, respectively.

Table 1. Maximum Sizes of the Solid Portion of Subsolid Nodules on Axial and MPR Images

Threshold (n = 25)	Mean Size (mm) ± Standard Deviation	Mean Difference (Bias)	p-Value
-100 HU			
Axial	0.26 ± 0.68	3.296	< 0.001
MPR	0.31 ± 0.87	3.247	< 0.001
-150 HU			
Axial	0.50 ± 0.94	3.057	< 0.001
MPR	0.55 ± 1.06	3.014	< 0.001
-200 HU			
Axial	0.89 ± 1.24	2.668	< 0.001
MPR	0.93 ± 1.31	2.630	< 0.001
-250 HU			
Axial	1.38 ± 1.58	2.182	< 0.001
MPR	1.39 ± 1.60	2.630	< 0.001
-300 HU			
Axial	1.88 ± 1.67	2.171	< 0.001
MPR	2.00 ± 1.67	1.565	< 0.001
-350 HU			
Axial	2.47 ± 1.88	1.094	0.002
MPR	2.76 ± 2.22	0.804	0.034
-400 HU			
Axial	3.17 ± 1.95	0.388	0.268
MPR	3.58 ± 2.39	-0.018	0.963
-450 HU			
Axial	4.07 ± 2.07	-0.514	0.142
MPR	4.52 ± 2.39	-0.962	0.011
-500 HU			
Axial	4.97 ± 2.17	-1.409	< 0.001
MPR	5.44 ± 2.47	-1.882	< 0.001
-550 HU			
Axial	6.25 ± 2.22	-2.693	< 0.001
MPR	6.67 ± 2.34	-3.109	< 0.001
-600 HU			
Axial	7.25 ± 2.50	-3.686	< 0.001
MPR	7.75 ± 2.56	-4.186	< 0.001

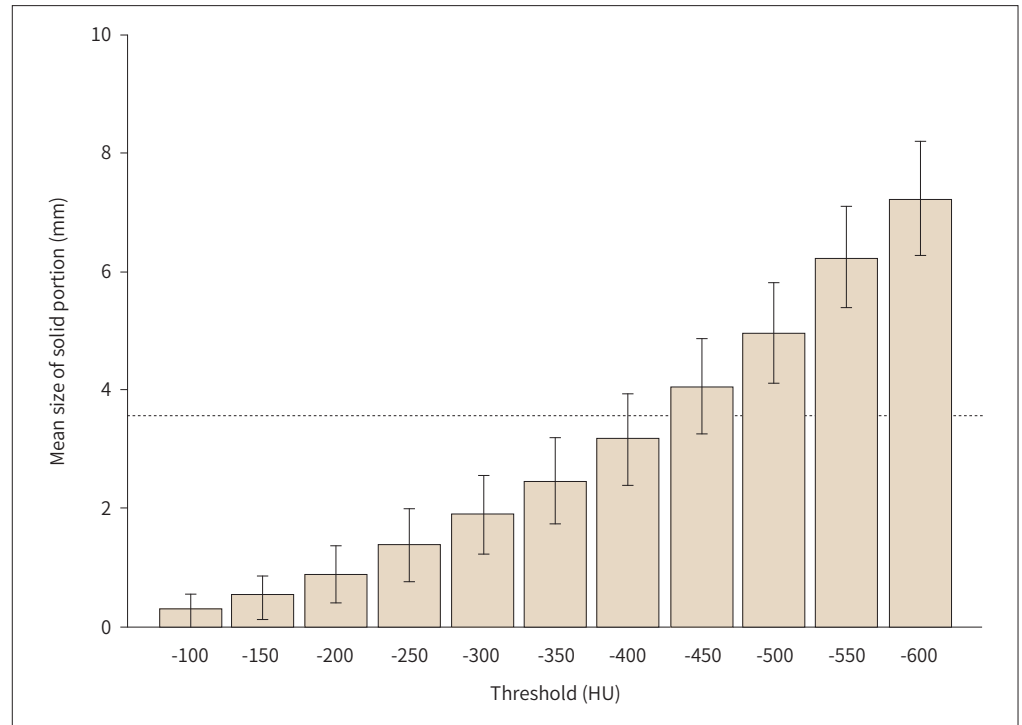
The mean size of pathologically confirmed invasive foci is 3.56 ± 1.33 mm.

HU = Hounsfield units, MPR = multiplanar reconstruction

CATEGORICAL ASSESSMENT

Radiologic classification of the 25 SSNs is summarized in Table 2 and Fig. 4. On both axial and MPR images, 25 pathologically proven MIA SSNs were categorized into 20 AIS and 5 MIA at -100 HU threshold and 4 MIA and 21 IA at -600 HU threshold. At a threshold of -400 HU on the axial image, 19 (76%) SSNs were classified into MIA, which showed the highest accuracy.

Fig. 2. Bar graph of bias between invasive foci and largest diameter of the solid portion on axial images along CT HU threshold with mean value and 95% confidence interval. The dotted line represents the mean size of pathologically confirmed invasive foci (3.56 mm). HU = Hounsfield units

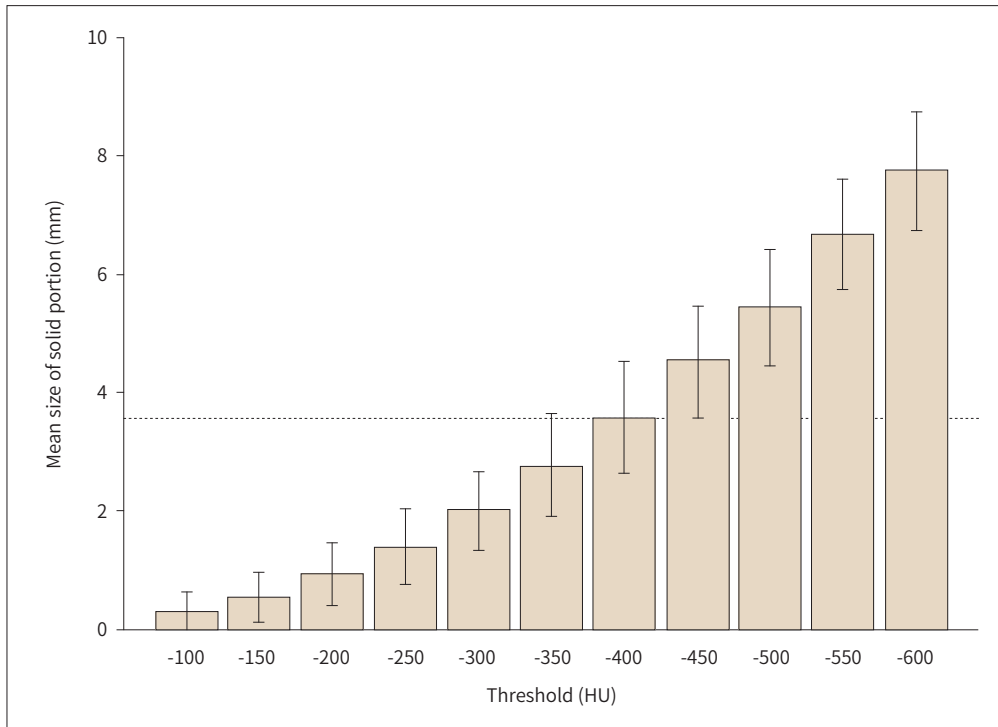


DISCUSSION

This study demonstrated that a threshold value which defines the solid component of MIA on the CT image of -400 HU showed the best performance. Both the largest diameter and the maximum diameter of the solid portion exhibited the lowest difference with the diameter of the pathologically confirmed solid portion on -400 HU, without significant difference. Bias was lower in the maximum diameter on the MPR image than in the largest diameter on the axial image. This finding may also be because the maximum diameter is measured in 3D dimension in pathology (14). However, -400 HU threshold on the axial image showed the highest accuracy for predicting MIA (76%). A threshold of -400 HU to -300 HU on both axial and MPR images showed relatively high accuracy for predicting MIA. As the threshold increased from -600 HU to -100 HU, the solid portion on CT reduced with increasing number of SSNs classified as AIS, indicating underdiagnosis. By contrast, as the threshold decreased from -100 HU to -600 HU, the solid portion on CT enlarged with increasing number of SSNs classified as IA, indicating overdiagnosis. Clinicians can use the lower HU threshold if they do not want to underdiagnosis the MIA as an AIS. Conversely, if clinicians do not want to overdiagnosis the MIA as an IA, they can use the relatively higher HU threshold.

In CT scan, the HU is proportional to the degree of X-ray attenuation (15), and attenuation of each pixel is related to tissue density (16). Normal alveolar structure and air space represent very low density, which is near -950–850 HU. However, as a tumor grows, cellularity in-

Fig. 3. Bar graph of bias between invasive foci and maximum diameter of the solid portion on multiplanar reconstruction images along CT HU threshold with mean value and 95% confidence interval. The dotted line represents the mean size of pathologically confirmed invasive foci (3.56 mm). HU = Hounsfield units



creases with high density and appears as high HU on CT, which is higher than the threshold, although it is difficult to differentiate with fibrosis, vasculatures, or the collapse of alveolar spaces (17, 18). According to the 2015 WHO classification, invasive foci of MIA are defined as either any histologic subtype other than a lepidic pattern (such as acinar, papillary, micropapillary, or solid) or tumor cells infiltrating myofibroblastic stroma (14). Thus, we can assume that the density or cellularity of invasive foci in SSNs may be higher than tissue density or cellularity of approximately -400 HU empirically as a result of this study, even though not exactly -400 HU, suggesting higher cellularity or density than non-invasive tumor lesion with lepidic cellular growth or normal structures.

Some studies expended effort to set HU threshold for the solid lesions of SSNs (11-13) and tend to suggest a relatively high HU value as threshold (11, 12). Matsuguma et al. (11) used -160 HU for the cut off value on the lung window to define the solid portion of SSNs. Similarly, Ko et al. (12) used -188 HU for the threshold and regarded the part of the nodule that showed higher attenuation as a solid part. The Fleischner guidelines recommended measurement of the solid component with narrow and/or mediastinal setting, which may indicate HU threshold near -150 HU considering the width and level of mediastinal setting (2, 19). Meanwhile, Cohen et al. (13) suggested that segmentation of the solid component shows the best performance at a threshold of -350 HU, and measurements on mediastinal windows (window width, 400 HU; level, 30 HU) were significantly smaller than the actual sizes of the invasive components. In the same context, Lee et al. (20) compared two different thresholds,

Table 2. Classification of SSNs by Size of the Solid Portion on CT

Threshold (n = 25)	AIS	MIA	IA
-100 HU			
Axial	20	5	0
MPR	20	5	0
-150 HU			
Axial	18	7	0
MPR	18	7	0
-200 HU			
Axial	14	11	0
MPR	14	11	0
-250 HU			
Axial	11	14	0
MPR	11	14	0
-300 HU			
Axial	7	18	0
MPR	7	18	0
-350 HU			
Axial	6	17	2
MPR	6	15	4
-400 HU			
Axial	2	19	4
MPR	2	15	8
-450 HU			
Axial	2	13	10
MPR	2	11	12
-500 HU			
Axial	0	13	12
MPR	0	9	16
-550 HU			
Axial	0	7	18
MPR	0	5	20
-600 HU			
Axial	0	4	21
MPR	0	4	21

AIS = adenocarcinoma in situ, HU = Hounsfield units, IA = invasive adenocarcinoma, MIA = minimally invasive adenocarcinoma, MPR = multiplanar reconstruction, SSNs = subsolid nodules

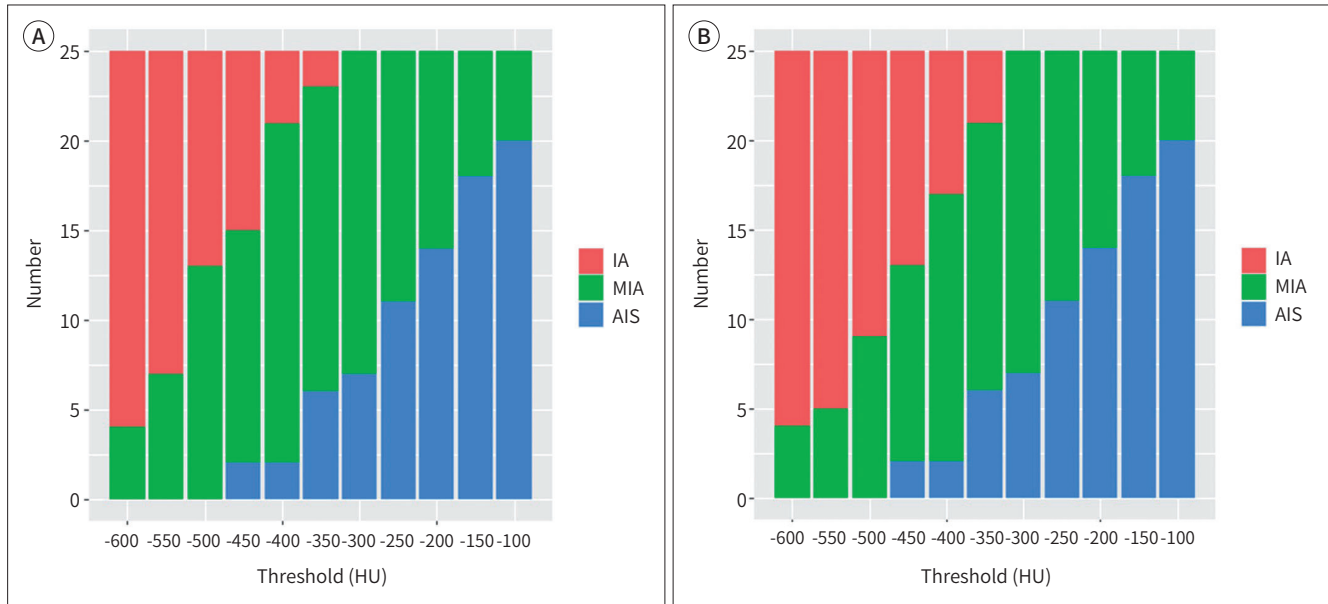
namely, -160 HU and -400 HU. They concluded high diagnostic accuracy in -400 HU for determining the presence of solid components of SSNs, whereas low sensitivity and negative predictive value in -160 HU. Similarly, we showed -400 HU as a threshold value for defining the solid component of SSNs. The high HU threshold is a conservative suggestion, which may overlook the actual solid portion; however, as in our suggestion with a lower threshold, it can be observed that it fits well.

Several recent technological approaches are available to analyze SSN characteristics by us-

Fig. 4. Stacked bar graph of 25 MIA SSNs for classification into radiologic AIS, MIA, and IA based on criteria for the measured solid portion on CT at each HU threshold.

A, B. Radiologic classification of the 25 SSNs, based on axial images (A) and multiplanar reconstruction images (B).

AIS = adenocarcinoma in situ, HU = Hounsfield units, IA = invasive adenocarcinoma, MIA = minimally invasive adenocarcinoma, SSNs = sub-solid nodules



ing CT textures, radiomics, or even artificial intelligence and deep learning (21-24). Chae et al. (21) reported that higher kurtosis is a significant differentiator of pre-invasive lesions from IA in SSNs. Son et al. (22) argued that the 75th percentile CT attenuation value and entropy can help distinguish them. Moreover, radiomics and deep learning have recently shown high performance in distinguishing IA along SSNs with an area under the curve more than 0.9 (23, 24). However, these complex methods are difficult to apply in daily practice, and further validation is needed. Our -400 HU threshold proposal is easy to apply as the default setting in PACS like the mediastinum setting, with excellent inter-observer agreement and high specificity for invasiveness, and even higher accuracy for real pathologically confirmed size of invasive foci.

This study has a number of limitations. First, it was a single-center retrospective study, and bias could not be avoided. Second, the study design only included pathologically confirmed MIA. No data were available for pre-invasive lesions, such as atypical adenomatous hyperplasia or AIS, and IA, and this can be considered as selection bias. Third, the sample size was small. A future multi-center study with large sample size involving other pre-invasive lesions is warranted. Finally, direct pathologic comparison was not conducted between CT showing solid portion and that exhibiting invasive foci of tissue. Solid portions of SSNs have a tendency to represent invasive foci, but they do not directly correspond with invasive foci (25). However, by setting a threshold attenuation of -400 HU for the solid portion of SSNs like in our study, the maximum diameter of the solid portion of SSNs can be easily and rapidly acquired without statistical difference with pathologically confirmed solid portion and with great inter-observer agreement.

In conclusion, -400 HU might be the optimal threshold to define the solid component of SSNs with the lowest bias and excellent inter-observer agreement. This threshold value is potentially helpful as a surrogate marker of invasive foci and to differentiate part-solid nodules from pure ground-glass nodules for guidelines.

Author Contributions

Conceptualization, L.S., L.D.H., K.T.H., P.C.H.; data curation, L.S., L.D.H., L.J.H.; formal analysis, H.K.; investigation, L.S., L.D.H., P.C.H., L.S.; methodology, L.S., L.D.H., K.T.H., P.C.H.; supervision, K.T.H., L.S.; visualization, L.S., K.T.H.; writing—original draft, L.S.

Conflicts of Interest

The authors have no potential conflicts of interest to disclose.

Funding

This study was supported by a faculty research grant of Yonsei University College of Medicine (6-2018-0060).

Acknowledgments

The scientific guarantor of this publication is Tae Hoon Kim (Department of Radiology and the Research Institute of Radiological Science, Gangnam Severance Hospital, Yonsei University College of Medicine).

Kyunghwa Han, an expert in statistics, provided statistical analysis and advice.

REFERENCES

- Hansell DM, Bankier AA, MacMahon H, McLoud TC, Müller NL, Remy J. Fleischner Society: glossary of terms for thoracic imaging. *Radiology* 2008;246:697-722
- MacMahon H, Naidich DP, Goo JM, Lee KS, Leung ANC, Mayo JR, et al. Guidelines for management of incidental pulmonary nodules detected on CT images: from the Fleischner Society 2017. *Radiology* 2017;284:228-243
- Heuvelmans MA, Oudkerk M. Management of subsolid pulmonary nodules in CT lung cancer screening. *J Thorac Dis* 2015;7:1103-1106
- American College of Radiology. Lung CT Screening Reporting & Data System (Lung-RADS), version 1.1. Available at: <https://www.acr.org/Clinical-Resources/Reporting-and-Data-Systems/Lung-Rads>. Published 2019. Accessed Mar 5, 2020
- Detterbeck FC, Boffa DJ, Kim AW, Tanoue LT. The eighth edition lung cancer stage classification. *Chest* 2017;151:193-203
- Travis WD, Brambilla E, Noguchi M, Nicholson AG, Geisinger KR, Yatabe Y, et al. International Association for the Study of Lung Cancer/American Thoracic Society/European Respiratory Society international multidisciplinary classification of lung adenocarcinoma. *J Thorac Oncol* 2011;6:244-285
- Lee HY, Lee KS. Ground-glass opacity nodules: histopathology, imaging evaluation, and clinical implications. *J Thorac Imaging* 2011;26:106-118
- Ridge CA, Yildirim A, Boiselle PM, Franquet T, Schaefer-Prokop CM, Tack D, et al. Differentiating between subsolid and solid pulmonary nodules at CT: inter- and intraobserver agreement between experienced thoracic radiologists. *Radiology* 2016;278:888-896
- Penn A, Ma M, Chou BB, Tseng JR, Phan P. Inter-reader variability when applying the 2013 Fleischner guidelines for potential solitary subsolid lung nodules. *Acta Radiol* 2015;56:1180-1186
- Kakinuma R, Ashizawa K, Kuriyama K, Fukushima A, Ishikawa H, Kamiya H, et al. Measurement of focal ground-glass opacity diameters on CT images: interobserver agreement in regard to identifying increases in the size of ground-glass opacities. *Acad Radiol* 2012;19:389-394
- Matsuguma H, Nakahara R, Anraku M, Kondo T, Tsuura Y, Kamiyama Y, et al. Objective definition and measurement method of ground-glass opacity for planning limited resection in patients with clinical stage IA

adenocarcinoma of the lung. *Eur J Cardiothorac Surg* 2004;25:1102-1106

12. Ko JP, Suh J, Ibdapo O, Escalon JG, Li J, Pass H, et al. Lung adenocarcinoma: correlation of quantitative CT findings with pathologic findings. *Radiology* 2016;280:931-939
13. Cohen JG, Goo JM, Yoo RE, Park CM, Lee CH, Van Ginneken B, et al. Software performance in segmenting ground-glass and solid components of subsolid nodules in pulmonary adenocarcinomas. *Eur Radiol* 2016; 26:4465-4474
14. Travis WD, Brambilla E, Nicholson AG, Yatabe Y, Austin JHM, Beasley MB, et al. The 2015 World Health Organization classification of lung tumors: impact of genetic, clinical and radiologic advances since the 2004 classification. *J Thorac Oncol* 2015;10:1243-1260
15. White S, Pharoah M. *Oral radiology: principles and interpretation*. 4th ed. St. Louis, MO: Mosby 2009:270-274
16. Gücük A, Uyetürk U. Usefulness of hounsfield unit and density in the assessment and treatment of urinary stones. *World J Nephrol* 2014;3:282-286
17. Aoki T, Hanamiya M, Uramoto H, Hisaoka M, Yamashita Y, Korogi Y. Adenocarcinomas with predominant ground-glass opacity: correlation of morphology and molecular biomarkers. *Radiology* 2012;264:590-596
18. Gandara DR, Aberle D, Lau D, Jett J, Akhurst T, Heelan R, et al. Radiographic imaging of bronchioloalveolar carcinoma: screening, patterns of presentation and response assessment. *J Thorac Oncol* 2006;1:S20-26
19. Naidich DP, Bankier AA, MacMahon H, Schaefer-Prokop CM, Pistolesi M, Goo JM, et al. Recommendations for the management of subsolid pulmonary nodules detected at CT: a statement from the Fleischner Society. *Radiology* 2013;266:304-317
20. Lee JH, Kim TH, Lee S, Han K, Byun MK, Chang YS, et al. High versus low attenuation thresholds to determine the solid component of ground-glass opacity nodules. *PLoS One* 2018;13:e0205490
21. Chae HD, Park CM, Park SJ, Lee SM, Kim KG, Goo JM. Computerized texture analysis of persistent part-solid ground-glass nodules: differentiation of preinvasive lesions from invasive pulmonary adenocarcinomas. *Radiology* 2014;273:285-293
22. Son JY, Lee HY, Lee KS, Kim JH, Han J, Jeong JY, et al. Quantitative CT analysis of pulmonary ground-glass opacity nodules for the distinction of invasive adenocarcinoma from pre-invasive or minimally invasive adenocarcinoma. *PLoS One* 2014;9:e104066
23. Luo T, Xu K, Zhang Z, Zhang L, Wu S. Radiomic features from computed tomography to differentiate invasive pulmonary adenocarcinomas from non-invasive pulmonary adenocarcinomas appearing as part-solid ground-glass nodules. *Chin J Cancer Res* 2019;31:329-338
24. Gong J, Liu J, Hao W, Nie S, Zheng B, Wang S, et al. A deep residual learning network for predicting lung adenocarcinoma manifesting as ground-glass nodule on CT images. *Eur Radiol* 2020;30:1847-1855
25. Lee KH, Goo JM, Park SJ, Wi JY, Chung DH, Go H, et al. Correlation between the size of the solid component on thin-section CT and the invasive component on pathology in small lung adenocarcinomas manifesting as ground-glass nodules. *J Thorac Oncol* 2014;9:74-82

폐의 아고형결절에서 침습적 병소를 검출하기 위한 반-정량 분석을 통한 최적의 CT 임계 값 결정

이선용¹ · 이다현¹ · 이재호¹ · 이성수² · 한경화³ · 박철환¹ · 김태훈^{1*}

목적 병리학적 침습성 병소를 기준으로 폐 아고형결절의 고형 부분을 진단하기 위한 최적의 CT 임계값을 알아보고자 하였다.

대상과 방법 병리적으로 최소 침습성 선암이 확진된 25명의 환자에 대해 비조영증강 흉부 CT 영상을 후향적으로 분석하였다. CT 영상에서 고형 부분은 -600부터 -100 Hounsfield units (이하 HU) 단위 사이에서 50 HU 간격의 다양한 임계치보다 높은 감쇠를 나타내는 영역으로 정의되었다. 각 임계치에서 고형부분의 축상 영상 최대 직경과 다면재구성 영상 최대 직경을 각각 측정 후, 선형 혼합 모델을 이용하여 병리적 침습성 병소 크기와 비교하였다.

결과 -400 HU 단위의 임계값에서 아고형결절의 고형 부분의 크기와 침습성 병소의 크기는 통계학적으로 유의미한 차이를 보이지 않았으며(축상 영상: $p = 0.2682$, 다면재구성 영상: $p = 0.963$) 오차가 가장 적었다(축상 영상: 0.388, 다면재구성 영상: -0.0176).

결론 아고형결절의 침습성 병소를 진단하기 위해, -400 HU 단위가 고형 부분을 정의하는 최적의 정량 분석 임계값일 수 있다.

¹연세대학교 의과대학 강남세브란스병원 영상의학과, 방사선외과학연구소,

²연세대학교 의과대학 강남세브란스병원 흉부외과,

³연세대학교 의과대학 세브란스병원 영상의학과